Anatomical and Optical Properties of Atrial Tissue: Search for a Suitable Animal Model

Narine Muselimyan, Mohammed Al Jishi, Huda Asfour, Luther Swift & Narine A. Sarvazyan

Cardiovascular Engineering and Technology

ISSN 1869-408X
Volume 8
Number 4

Cardiovasc Eng Tech (2017) 8:505-514
DOI 10.1007/s13239-017-0329-7

Springer

Cardiovascular Engineering and Technology, Vol. 8, No. 4, December 2017 (© 2017) pp. 505–514
DOI: 10.1007/s13239-017-0329-7

Anatomical and Optical Properties of Atrial Tissue: Search for a Suitable Animal Model

NARINE MUSELIMYAN, MOHAMMED AL JISHI, HUDA ASFOUR, LUTHER SWIFT, and NARINE A. SARVAZYAN

Department of Pharmacology and Physiology, The George Washington University School of Medicine and Health Sciences, 2300 Eye Street NW, Washington, DC 20052, USA

(*Received 9 May 2017; accepted 28 August 2017; published online 7 September 2017*)

Associate Editor Peter E. McHugh and Ajit P. Yoganathan oversaw the review of this article.

Abstract—The purpose of this study was to evaluate structural and optical properties of atrial tissue from common animal models and to compare it with human atria. We aimed to do this in a format that will be useful for development of better ablation tools and/or new means for visualizing atrial lesions. Human atrial tissue from clinically relevant age group was compared and contrasted with atrial tissue of large animal models commonly available for research purposes. These included pigs, sheep, dogs and cows. The presented data include area measurements of smooth atrial surface available for ablation and estimates of thickness of collagen and muscle for five different species. We also described methods to quantify presence of collagen and overall thickness of atrial wall. Provided information enables placement of atrial lesions to locations with clinically relevant atrial wall thickness and macroscopic structure ultimately helping investigators to develop better ablation and imaging tools. It also highlights the impact of collagen thickness on optical measurements and lesion visualization.

Keywords—Catheter development, Atrial tissue, Spectroscopy, Collagen, Ablation lesions, Atrial fibrillation.

ABBREVIATIONS

AF	Atrial fibrillation
CCD	Charge-coupled device
LA	Left atria
RA	Right atria
RF	Radiofrequency
VVG	Verhoeff-van Gieson
OD	Optical density

Address correspondence to Narine A. Sarvazyan, Department of Pharmacology and Physiology, The George Washington University School of Medicine and Health Sciences, 2300 Eye Street NW, Washington, DC 20052, USA. Electronic mail: phynas@gwu.edu

Disclosures N. Sarvazyan reports a patent application filed by the George Washington University that is related to use of hyperspectral imaging for atrial fibrillation treatment. She also holds stock options in LuxCath LLC. The rest of the authors have no relevant financial interests and no potential conflicts of interest to disclose.

INTRODUCTION

Atrial fibrillation (AF) remains the most common cardiac arrhythmia.[3] Hundreds of thousands of patients undergo ablation procedures to treat this potentially life-threatening condition since it greatly increases the likelihood of stroke and ventricular fibrillation.[26,28] Yet as of today, percutaneous ablation of AF sources is done in a 'blind' fashion due to the absence of imaging tools to identify the boundaries of ablated tissue and depth of ablation lesions. The remaining gaps in ablation lines and secondary arrhythmic triggers can then contribute to recurrence of AF *via* breaks in intended conduction block.[2,14] As a result, at least one-third of AF patients need to return for repeat procedures.[27,33]

To improve the efficacy of AF treatment multiple groups, including ours, are developing new types of intracardiac catheters. These new catheters aim to either create deeper and more contiguous lesions and/or to image, in real time, ablation induced necrosis of atrial tissue. These new imaging methods include, among others, optical coherence tomography,[11] photoacoustics,[7] hyperspectral imaging,[12,25] polarization spectroscopy[1] and autofluorescence measurements.[19,31] To test these new techniques, animal analogs of human tissue of interest have to be employed. It then becomes critical to know what aspects of that chosen animal model are similar to the human tissue and which ones are different. Unfortunately, such information is either scattered thru the literature or is not available. Specifically, to the best of our knowledge, no system-

atic studies have compared structural and optical properties of different animal models of atrial tissue and their relationship to human atria in a format that would help investigators develop novel ablation tools and visualize atrial lesions.

To address this need, we compared and contrasted human atrial tissue from clinically relevant age group with atrial tissue of large animal models commonly available for research purposes. These included freshly excised samples from pigs, sheep and cows, all of which can be readily acquired from a local abattoir. We also included atrial tissue of pigs and mongrel dogs after surgical training. The latter is rarely approved for the sole purpose of methodological testing, yet canine atria can become available upon the completion of an unrelated terminal surgical procedure conducted in the same research institution.

MATERIALS AND METHODS

Tissue Sources

The animal specimens were obtained from a local abattoir or upon completion of surgical training at the George Washington University Washington Institute of Surgical Education (WISE) in full compliance with institutional animal use and care committee protocols. Animal tissues were acquired from ostensibly healthy subjects. Each specimen had been preserved in ice-cold isotonic saline. Donated human hearts were procured from Washington Regional Transplant Community (WRTC, Washington, DC) which maintains its own IRB protocol. Explanted hearts were cardioplegically arrested, cooled to +4 °C in the operating room following aortic cross-clamp and transported to the laboratory on ice. Hearts were cut from the great vessels and pericardium, with special care to leave most of the atria intact. Fat tissue was carefully removed from the epicardial surface in order to lay atria flat. The left and right atria were dissected along the atrioventricular groove, and along the interatrial septum. This allowed for the inversion of the tissue, thereby exposing the endocardial surface. The atria were then spread out for imaging and other measurements.

Histology and Gross Pathology

Atria are highly heterogeneous, therefore for quantitative comparison, histological specimens were taken from the same area across all species, specifically from left atrial roof. Tissue was fixed in 10% neutral buffered formalin solution, embedded in paraffin, sectioned into 4μm slices and stained with hemotoxylin/eosin and VVG (Verhoeff-van Gieson) stains according to standard pathology protocols. Processed slices were then imaged using an Axiovert 105 camera mounted on a Primovert Zeiss scope. Zen (Zeiss Inc, Germany) software was used to measure the thickness of the atria wall, including its muscle and collagen layer.

Imaging Protocols

Samples were photographed under either incandescent light or a UV light source (365 nm LED spotlight 500 mA power, Mightex, Pleasanton, CA). Radiofrequency (RF) energy was delivered with a non-irrigated ablation catheter (EP Technologies, Boston Scientific). To acquire hyperspectral images, a Nuance FX HSI system (PerkinElmer/Cri, Waltham, MA), was used. It is comprised of a camera lens (Nikon AF Micro-Nikkor 60 mm f/2.8D Lens), liquid crystal tunable filter (CRi LCTF), and a monochromatic charged-coupled device (Sony ICX285 CCD). For trans-illumination experiments, dissected atrial tissue was placed on top of an LED light box with a flat surface and diffuse white light source beneath. Images were acquired at 720 nm emission settings using Nuance FX Optical Density (OD) mode settings. Image processing and intensity quantification was done using NIH ImageJ software.

RESULTS

Animal and Human Samples

Three to six hearts from each species were used to derive qualitative and quantitative conclusions detailed in this paper. Abattoir specimens included hearts from cows ($n = 5$, mixed gender, 22–24 month-old, 1200–1500 lb body weight), pigs ($n = 5$, mixed sex, 6–7 month-old, Yorkshire breed, 300–400 lb body weight), and lamb ($n = 5$, mixed sex, 6–7 month-old, Dorper breed, 80–85 lb body weight). Animal hearts analyzed upon completion of terminal surgery for unrelated protocols at our research institution included smaller pigs ($n = 5$, mixed sex, 4–5 month old, Yorkshire-Hampshire hybrid, 50–60 lb) and dogs ($n = 4$, mongrel, female, 10–14-month old, 45–55 lb body weight). Six human hearts from deceased individuals were received from a local donor bank (mixed sex, 68 ± 10 years old). Values are presented as mean ± SEM unless noted otherwise, with Student's t test values of $p < 0.05$ considered significant.

Anatomical Differences on the Whole Heart Level

We would like to re-emphasize that this is not a comparative anatomy study in its true sense since we

examined atria from different species within different age groups. Instead, we acquired animal hearts from local abattoir sources or after completion of surgical training and compared them with samples of human atria from patients within an age group most likely to be affected by AF.[6] Figure 1 show representative images which illustrate major size and shape differences between hearts from five species. The epicardial surface of aged human hearts is largely covered by adipose tissue. Bovine and ovine hearts also exhibit significant amount of epicardial fat, while porcine and canine hearts have less. The color of fat on the surface of human heart is much more yellow compared to other examined species. The shape of human and canine heart is typically more trapezoidal, while hearts from quadruped mammals (cow, pig and sheep) are more elongated with a pointed apex. The apex of each species is a left ventricular structure.

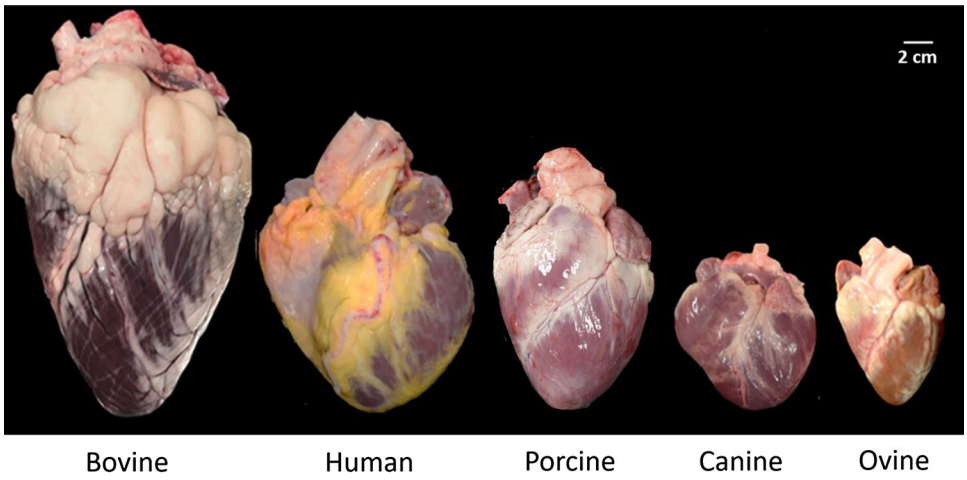

FIGURE 1. Examples of visual appearance of excised hearts from five different species considered in this article. From left to right: cow, human, pig, dog, lamb. Bar—2 cm.

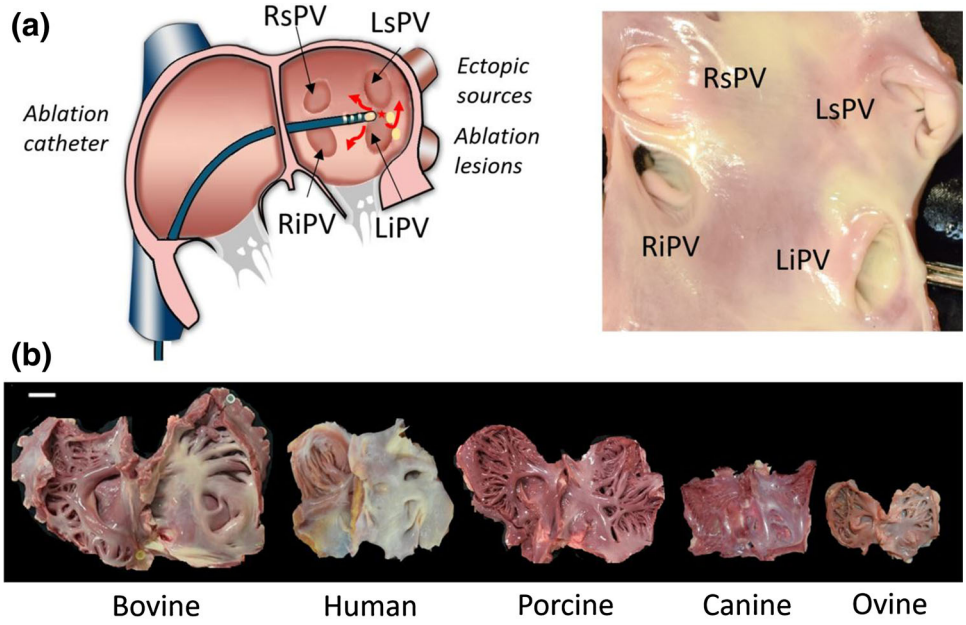

FIGURE 2. Cartoon of typical RF ablation procedure and the visual appearance of excised atria. (a) A cartoon showing insertion of a percutaneous catheter from the inferior vena cava and foramen ovale into the LA. Ectopic sources (red arrows) are then ablated (yellow dots) near the entrance of four pulmonary veins (RiPV stands for right inferior pulmonary vein, RsPV – right superior pulmonary vein, LiPV and LsPV- left inferior and right superior pulmonary veins respectively). On the right is the excised and flattened surface of a human LA showing its pale and smooth endocardial surface; (b) The visual appearance of excised and flattened atria from five different species. Bar—2 cm.

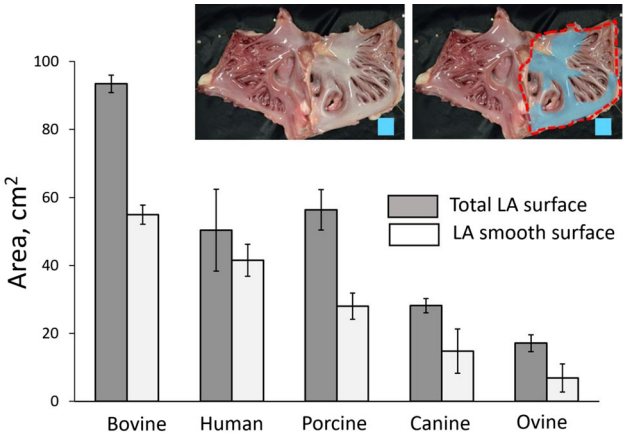

FIGURE 3. Measurements of the total vs. pectinate muscle-free surface area of excised LA. The top images show example of porcine atria and the way the total and trabeculation-free areas of LA were outlined. Scale box—4 cm^2.

Atrial Anatomical Differences

A vast majority of AF triggers are believed to originate from left artium (LA) sources, particularly near orifices of pulmonary veins.[14] Therefore, the most common AF ablation procedure involves creating ablation lines around pulmonary veins to isolate those triggers from the rest of the atrial tissue (Fig. 2a, left panel). In humans, the endocardial LA surface near the entrance to the pulmonary veins is largely free from trabeculations created by pectinate muscles (Fig. 2a, right panel). This makes applying a contiguous ablation line relatively straightforward. However, one often faces a challenge creating similar lesions in animal models, since the size of an available smooth endocardial surface in animal hearts is much more limited—on either left or right side of the atrium (Fig. 2b). We quantified the size of smooth surface available for

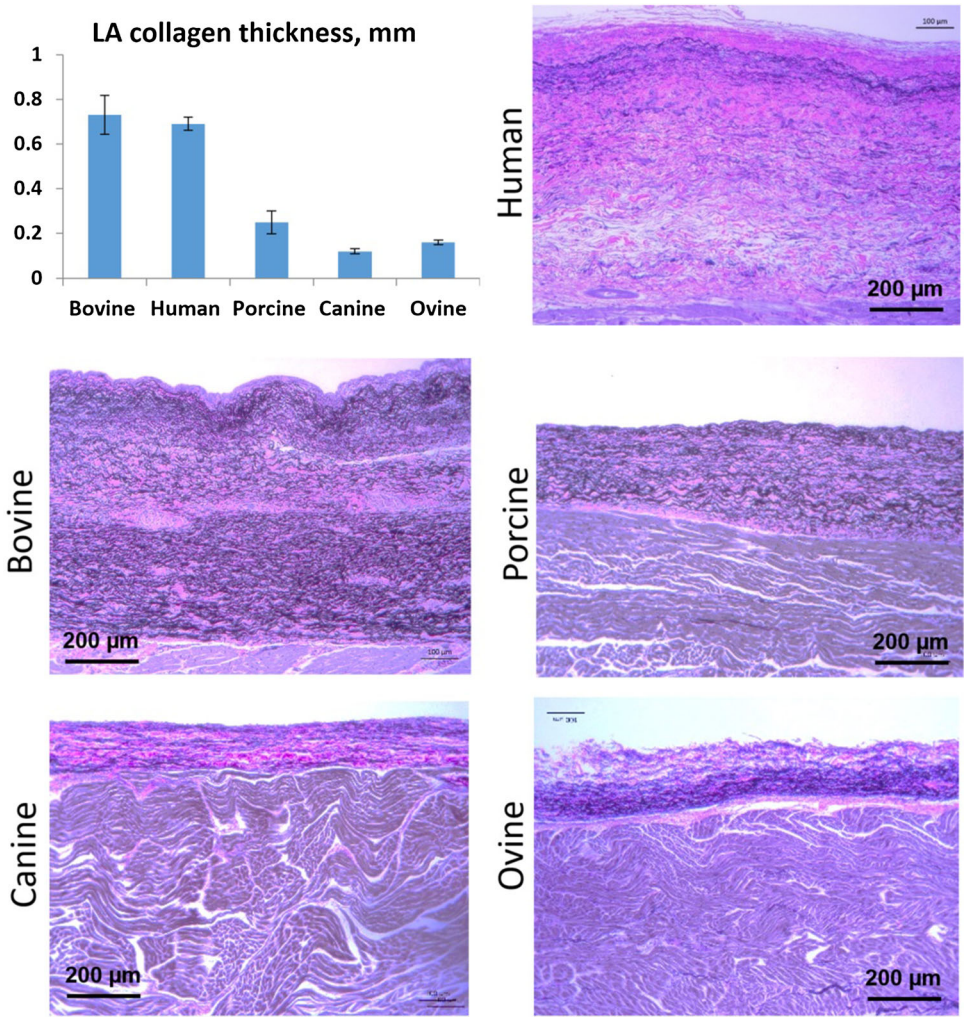

FIGURE 4. Measurements of collagen layer thickness. Values are from LA roof. Representative histology slices stained with VVG stain are shown. Pink represents collagen, black—elastin, purple—muscle.

ablation experiments by outlining the total and the trabeculated areas of pectinate muscles in LA using ImageJ tools in each of the examined species (Fig. 3).

The total surface area of the RA was comparable to that of the LA across all species (Fig. 2b). However, due to its highly trabeculated nature the RA is much less suitable for catheter testing. The latter is not much of a concern because clinically AF ablation mainly targets LA sources. RA and LA also differs when it comes to the composition of the atrial wall as detailed below. Lastly, it is worth mentioning that the number of pulmonary veins varies between species. Humans usually have four pulmonary veins, pigs 2 and dogs 5–6. A comparison of other gross differences in atrial morphology and anatomy can be found elsewhere.[16]

Collagen Lining of Atrial Surface and Tools to Map It

Visual observation of endocardial surfaces enables easy identification of LA and RA by their color (Fig. 2b). A much whiter color of the LA endocardial surface is due to the presence of a thicker collagen layer. From the point of designing and interpreting animal experiments one should keep in mind that the main goal of AF ablations is to destroy electrically active muscle beneath the collagen layer. The physical properties of collagen are quite different from that of muscle, so it is critical to consider how much collagen is present in animal models compared to that of humans. Figure 4 illustrates the relative thickness of collagen from histology slides of samples taken from the LA roof of each species. The thickness of the collagen layer was found to be ~0.6 mm in aged humans, which was similar to the samples taken from the LA of 2-year old cows. In contrast, in all other examined species LA collagen layer that was 3–5 times thinner. The collagen layer in cows also contained the largest amount of elastin. The latter has a spring-like appearance on VVG stained samples (Fig. 4, middle left panel).

Thickness values shown in Fig. 4 were derived from multiple individual measurements of the atrial wall using histology slices of LA roof samples. Considering that roof makes up only a small portion of the LA, these measurements can be viewed only as a first approximation for cross-species comparison purposes. In fact, the thickness of the LA collagen layer varies

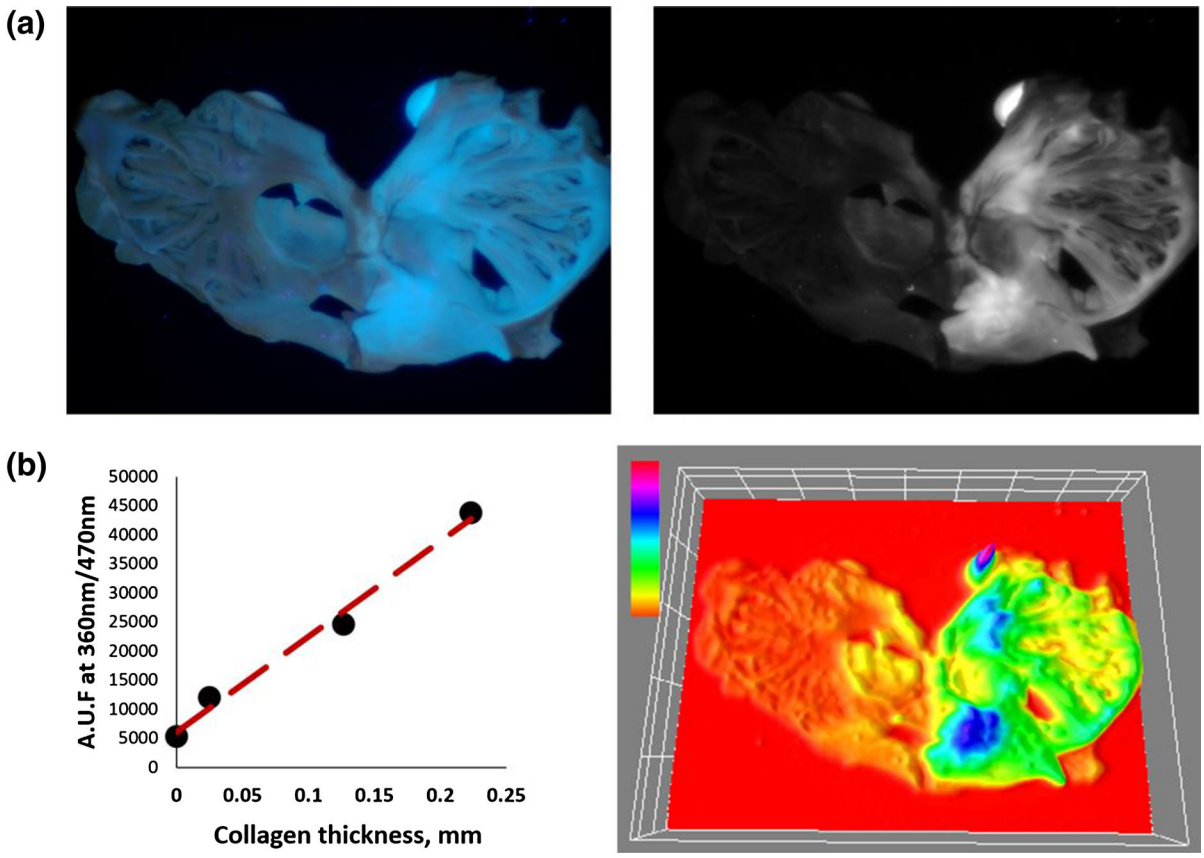

FIGURE 5. Macroscopic determination of endocardial collagen thickness. (a) Left image shows the visual appearance of ovine atria under illumination with a 365 nm LED light source. The right image is the same specimen but acquired at a 470 nm wavelength. (b) The linear relationship between the thickness of collagen layer and autofluorescence intensity at 470 nm is shown on the right. Next to it is a color map of collagen thickness for the entire atria based on the linear calibration curve.

greatly throughout the atria. Therefore, to properly design and interpret ablation experiment done at the bench, it useful to know the distribution of collagen before the actual ablation. Since collagen is highly autofluorescent, this information can be obtained using relatively simple and affordable optical tools. To obtain a map of collagen distribution and thickness, flattened atria can be illuminated with a 350–390 nm light using either commercial or common marketplace light sources (i.e., 385~395 nm LED flashlight). The intensity of the autofluorescence acquired at 400–470 nm wavelength range is directly proportional to the thickness of collagen layer (up to 1 mm thickness). An example of such measurements is included in Fig. 5. It shows the visual appearance of an ovine atria illuminated with a 365 nm LED light source and a corresponding image at 470 nm, revealing the collagen distribution. To obtain a calibration curve one needs to excise several small atrial wall samples, acquire intensity of autofluorescence signals and plot them against respective collagen thickness of these samples determined from histological assessment. The exact values will depend on the user's light source and camera settings, therefore arbitrary units are shown on the y-axis. A macroscopic map of collagen thickness throughout the entire atria can then be produced and displayed using either 3D mesh, or pseudocolor, or both (Fig. 5, bottom right).

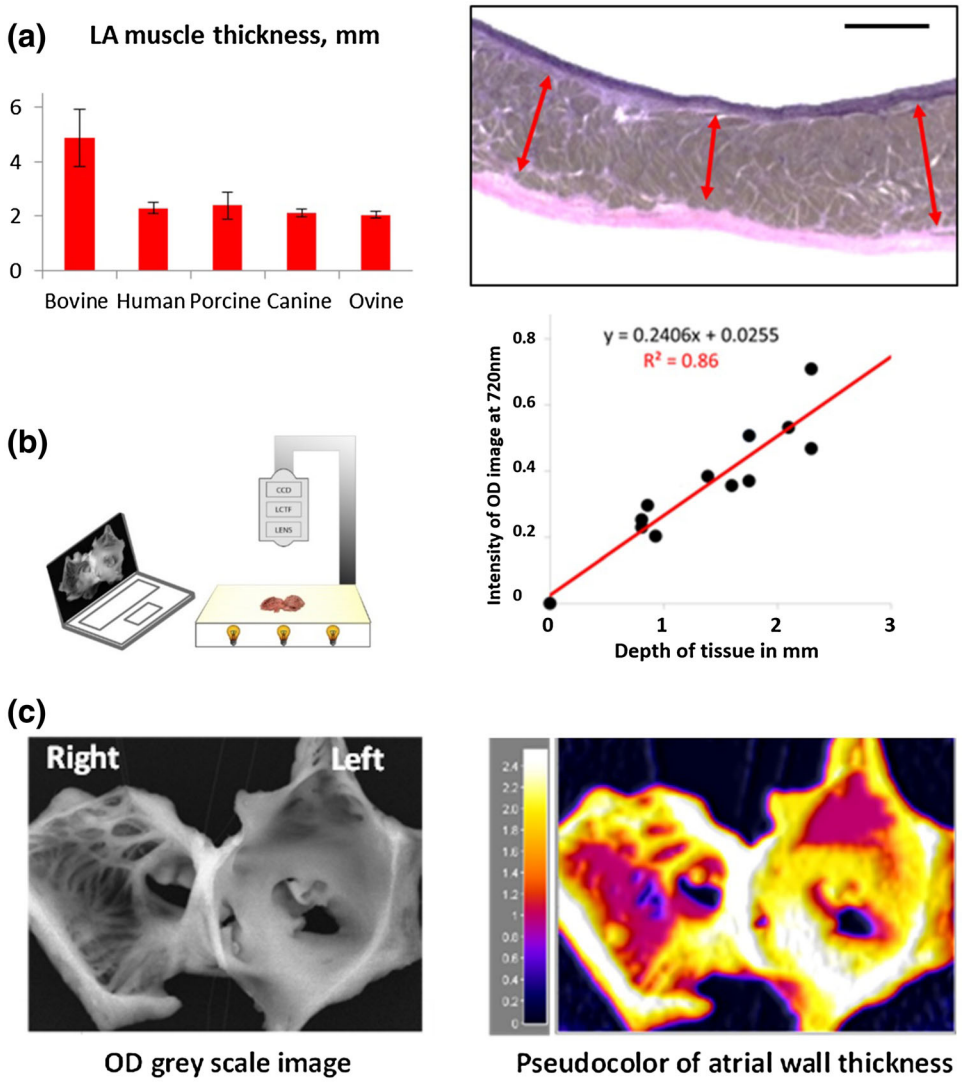

FIGURE 6. Measurements of LA muscle thickness and macroscopic determination of atrial wall thickness. (a) Left panel displays the values of muscle layer thickness from the roof the LA and a representative porcine histology sample stained with hematoxylin–eosin stain next to it; (b) A cartoon of transmittance setup and the calibration curve next to it showing linear relationship between optical density of transmitted 720 nm light and the thickness of excised atrial samples; (c) The bottom panels are examples of a grey scale transmittance image of canine atria and the corresponding pseudocolor map of its thickness.

Atrial Wall Thickness and Tools to Map It

The ultimate target of AF ablation is atrial muscle. To compare its thickness across the species, we derived muscle thickness values from multiple discrete measurements of the atrial wall using histology slices of LA roof samples (Fig. 6a). Interestingly, the thickness of human LA muscle was comparable to that of canine, porcine and ovine hearts, although these hearts were smaller in size (Fig. 1). Human atria were thinner than bovine samples, the latter reaching 7–8 mm in its thickness.

The atrial wall thickness, in its first approximation, is a sum of muscle and collagen thickness. It varies greatly throughout the atria. To obtain a macroscopic map of atrial wall thickness, flattened atria can be placed on top of an X-ray viewer (or any type of light box with a diffuse broadband white light source beneath), while near infrared (IR) signals are recorded with a camera equipped with either a tunable filter or a IR bandpass. The log intensity of passing light intensity is inversely proportional to tissue thickness up to 4–5 mm. The latter value is close to the upper limit of LA thickness in all examined species except cow. Figure 6b shows experimental data validating this simple yet effective approach by plotting optical density (OD) values of several regions of interests vs. micrometer-based measurements of canine wall thickness. By creating a calibration curve for their specific light source, bandpass filter and the camera, one can then derive the average left or right wall thickness, its minimal and maximum values as well as display it using either a pseudocolor or a 3D mesh (Fig. 6c). Based on our experience, any bandpass filter within 700–900 nm range provided a good first order estimate of atrial tissue wall thickness.

Age and Breed Variability

The presented images and values are typical examples for commonly available market age animals. Yet it is important to emphasize that age, sex and specific breed of the animal will have significant impact on these values. For example, in previous figures we considered atrial tissue from porcine hearts obtained from a local abattoir (~7-month-old, 150–200 kg Yorkshire pigs). The weights of their hearts and excised atria were 434 ± 51 g and 77 ± 6 respectively. When we compared them to the hearts and excised atrial tissue from pigs used for surgical training at GW Institute for Surgical Education (~4 month-old, 50–60 kg, Hampshire-Yorkshire hybrid), their values were expectably lower (153 ± 14 and 30 ± 3 g for the heart and excised atria respectively). Notably, heart-to-body weight ratio, percentage of non-trabeculated smooth LA surface as well as thickness of collagen layer were not significantly different (Fig. 7).

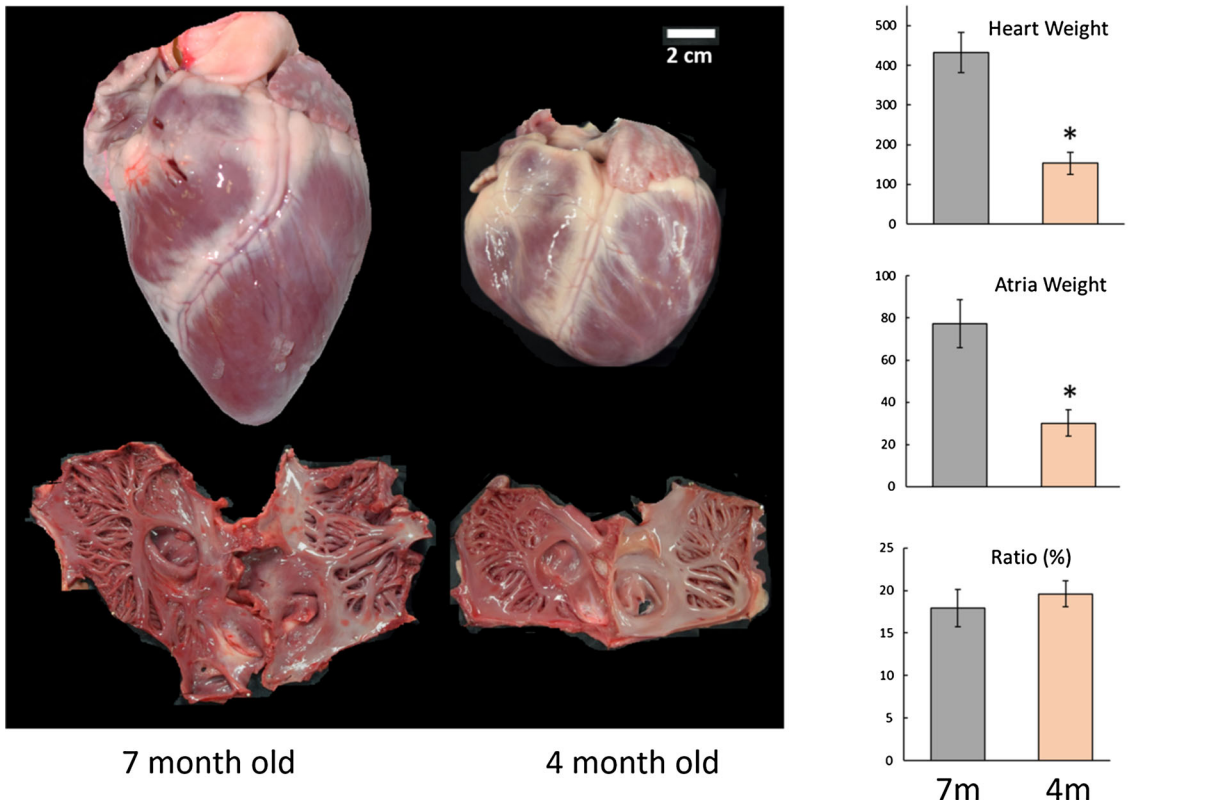

FIGURE 7. Effect of animal breed and age. Images and graphs illustrate the differences between hearts from 7-month-old pigs vs. smaller, 4 month old pigs used for surgical testing.

Optical Changes Caused by Radiofrequency Ablation

When RF ablation is performed on the surface of ventricular muscle, the lesion is readily visible under both incandescent light or UV illumination settings (Fig. 8a). For the atrial tissue, however, the abundance of the highly reflective and autofluorescent collagen layer obscures the underlying muscle damage. An example of a typical appearance of an ablated bovine LA endocardial surface with sites of radiofrequency ablation lesions barely detectable by eye is shown in Fig. 8b (left and middle panels). Fortunately, more advanced optical approaches can often help to reveal lesion boundaries and even depth.[1,12,25,30] One such approach is hyperspectral imaging which exploits small differences between autofluorescence spectrum of ablated and unablated atrial tissue (Fig. 8b right panel, details in Refs. 1, 12, 25).

DISCUSSION

AF remains one of the most significant health burdens and is expected to affect over 12 million people in the United States by 2050.[3] The incidence of AF continues to rise due to the aging of the world's population.[18] The most common and effective way to treat drug-resistant AF is surgical ablation of arrhythmogenic sources.[21,28] AF ablation is performed using percutaneous ablation catheters that use different physical means to destroy or electrically isolate tissue from which sources of abnormal activity are detected.[23] The vast majority of these sources have been shown to arise from left atrial muscle near orifices of pulmonary veins.[14] Surgical ablation can be a very effective way to treat AF, yet in about third of the cases a patient needs to have repeat ablation procedures due to return of AF.[27]

Multiple groups,[1,7,15,22,30] including ours,[12,25,31] continue to search for ways to improve outcomes of AF ablation procedures, so it can be done faster and with a lower incidence of repeat procedures. These efforts include the development of new tools to create deeper and more continuous lesions with greater precision [4,8,9] as well as novel means for in-surgery visualization of the lesions.[1,7,10,13,20,24] To test these new protocols and techniques, researchers must ablate tissue that will be analogous to their future clinical target. Yet, today there is a paucity of published information regarding features of atrial tissue from readily available animal sources vs. what will be a clinical target for

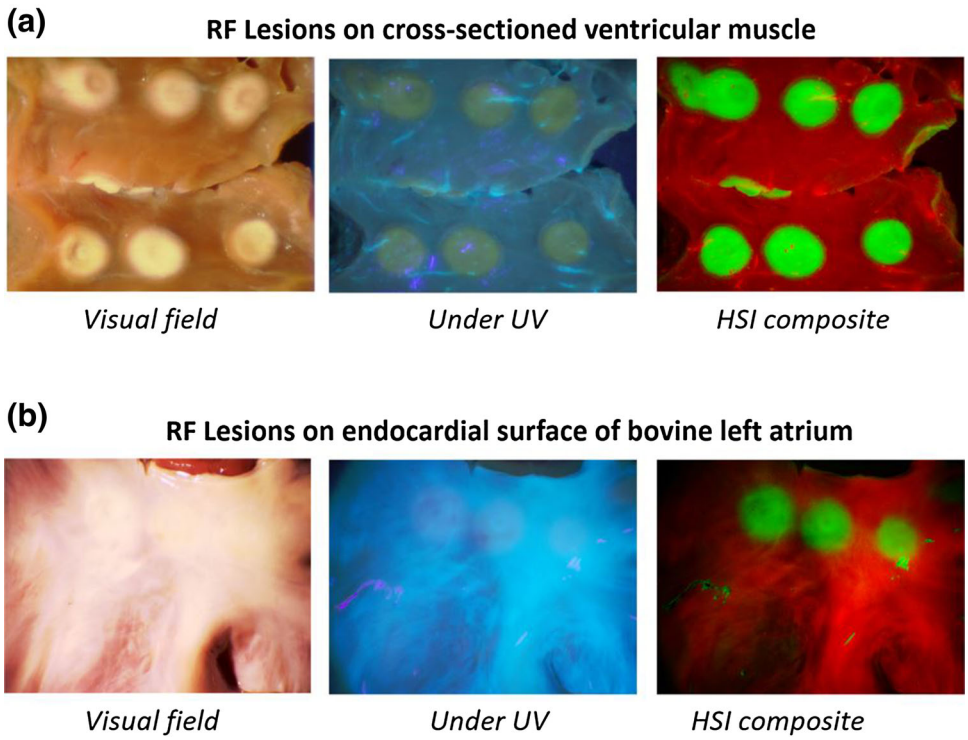

FIGURE 8. Differences in the visual appearance of RF lesions made on ventricular muscle vs. LA endocardium. (a) Unstained surface of ventricular slab with multiple RF lesions under either room light or UV illumination. RF ablation causes muscle to turn pale and lose its NADH (the latter makes tissue markedly more yellow under UV illumination). Use of hyperspectral imaging (right column) enables clear classification of tissue as ablated (green) or unablated (red); (b). Unstained endocardial surface of bovine LA with multiple RF lesions under either room light or UV illumination. Note the limited contrast between the lesions and unablated, healthy tissue due to the abundance of endocardial collagen. Use of hyperspectral imaging (right column) enables clear classification of tissue as ablated (green) or unablated (red).

AF ablation surgery. The few comparative papers we found were focused on different animal models of AF or on anatomical differences of the atria relevant to xenotransplantation procedures or use of porcine valves.[5,16]

Our comparative studies of animal and human atria had a very specific goal of providing essential basic information for the proper design of ablation catheter testing using animal tissue. It did not delve into the complex arrangement of fiber bundles within the muscle wall,[17,29] or intricate structure of endocardial collagen layer, which also contains large amount of elastin, smooth muscle cells, fat and other components.[32] In our first-degree approximation, we also ignored effects that animal gender, age or breed will have on reported values. Yet, this is something that obviously should be taken into account as illustrated in Fig. 7.

We want to highlight an important difference between the appearance and properties of RF lesions placed on ventricular vs. atrial tissue (Fig. 8, images on the left). The endocardial surface of left atria is covered with a dense collagen layer. Being highly reflective and fluorescent, collagen largely masks sites of thermal injury to the muscle below, affecting the way light interacts with the surface of tissue to be ablated. Collagen's other physical properties, including impedance, velocity of sound, shear wave elasticity, light polarization also differ from that of a muscle. Yet unfortunately, today most of ablation and imaging techniques intended to be used for atrial tissue are often being tested using trimmed wedges of ventricular muscle. The presented data clearly shows that this key structural difference between the atrial and ventricular tissue must be taken into account.

The presented data offers a range of useful information for anyone who is planning bench testing of new ablation protocols or examining novel devices. This includes area measurements of smooth atrial surface available for ablation and estimates of thickness of collagen and muscle for five different species. We also described an affordable and easy way to visualize the abundance of collagen and the overall thickness of atrial tissue. This can significantly improve placement of atrial lesions onto locations which have clinically relevant wall thickness and structure. It can also improve translatability of animal testing of AF treatment tools and methods of detection and visualization of ablation lesions.

ACKNOWLEDGMENTS

We gratefully acknowledge Christian Lefever, MD for helpful discussions and editorial suggestions.

CONFLICT OF INTEREST

N. Sarvazyan reports a patent application filed by the George Washington University that is related to use of hyperspectral imaging for atrial fibrillation treatment. She also holds stock options in LuxCath LLC. The rest of the authors have no relevant financial interests and no potential conflicts of interest to disclose.

FUNDING

This study was funded by the National Institutes of Health R42 HL120511 award.

ETHICAL APPROVAL

All applicable international, national, and/or institutional guidelines for the care and use of animals were followed. This article does not contain any studies with human participants performed by any of the authors. Donated human hearts were procured from Washington Regional Transplant Community (WRTC, Washington, DC) which maintains its own IRB protocols.

REFERENCES

[1]Ahmad, I., A. Gribble, M. Ikram, M. Pop, and A. Vitkin. Polarimetric assessment of healthy and radiofrequency ablated porcine myocardial tissue. *J. Biophotonics*. 9(7):750–759, 2016.

[2]Baykaner, T., P. Clopton, G. G. Lalani, A. A. Schricker, D. E. Krummen, and S. M. Narayan. Targeted ablation at stable atrial fibrillation sources improves success over conventional ablation in high-risk patients: a substudy of the CONFIRM Trial. *Can. J. Cardiol*. 29(10):1218–1226, 2013.

[3]Benjamin, E. J., *et al*. Heart disease and stroke statistics-2017 update: a report from the American Heart Association. *Circulation* 135(10):e146–e603, 2017.

[4]Boersma, L. V., M. C. Wijffels, H. Oral, E. F. Wever, and F. Morady. Pulmonary vein isolation by duty-cycled bipolar and unipolar radiofrequency energy with a multi-electrode ablation catheter. *Heart Rhythm* 5(12):1635–1642, 2008.

[5]Bourne, G. Hearts and heart-like organs: comparative anatomy and development. Cambridge: Academic Press Inc, 1981.

[6]Chen, H.-Y., *et al*. A 35-year perspective (1975 to 2009) into the long-term prognosis and hospital management of patients discharged from the hospital after a first acute myocardial infarction. *Am. J. Cardiol*. 116(1):24–29, 2015.

[7]Dana, N., L. Di Biase, A. Natale, S. Emelianov, and R. Bouchard. In vitro photoacoustic visualization of myocardial ablation lesions. *Heart Rhythm* 11(1):150–157, 2013.

[8]Defaye, P., A. Kane, A. Chaib, and P. Jacon. Efficacy and safety of pulmonary veins isolation by cryoablation for the treatment of paroxysmal and persistent atrial fibrillation. *Europace* 13(6):789–795, 2011.
[9]Dukkipati, S. R., *et al*. Pulmonary Vein Isolation Using the Visually Guided Laser Balloon. *J. Am. Coll. Cardiol.* 66(12):1350–1360, 2015.
[10]Fleming, C. P., K. J. Quan, and A. M. Rollins. Toward guidance of epicardial cardiac radiofrequency ablation therapy using optical coherence tomography. *J. Biomed. Opt*. 15(4):41510, 2010.
[11]Gan, Y., D. Tsay, S. B. Amir, C. C. Marboe, and C. P. Hendon. Automated classification of optical coherence tomography images of human atrial tissue. *J. Biomed. Opt*. 21(10):101407, 2016.
[12]Gil, D., L. M. Swift, H. Asfour, N. Muselimyan, M. A. Mercader, and N. Sarvazyan. Autofluorescence hyperspectral imaging of radiofrequency ablation lesions in porcine cardiac tissue. *J. Biophotonics*. 10:1008–1017, 2017.
[13]Granier, M., *et al*. Real-time atrial wall imaging during radiofrequency ablation in a porcine model. *Heart Rhythm* 12(8):1827–1835, 2015.
[14]Haıssaguerre, M., *et al*. Spontaneous initiation of atrial fibrillation by ectopic beats originating in the pulmonary veins. *N. Engl. J. Med.* 339(10):659–666, 1998.
[15]Herranz, D., J. Lloret, S. Jimenez-Valero, J. L. Rubio-Guivernau, and E. Margallo-Balbas. Novel catheter enabling simultaneous radiofrequency ablation and optical coherence reflectometry. *Biomed. Opt. Express*. 6(9):3268–3275, 2015.
[16]Hill, A. J., and P. A. Iaizzo. Comparative Cardiac Anatomy. In: Handbook of Cardiac Anatomy, Physiology, and Devices, edited by P. A. Iaizzo. Cham: Springer International Publishing, 2015, pp. 89–114.
[17]Ho, S. Y., R. H. Anderson, and D. Sanchez-Quintana. Atrial structure and fibres: morphologic bases of atrial conduction. *Cardiovasc. Res*. 54(2):325–336, 2002.
[18]Kitzman, D. W., and W. D. Edwards. Age-related changes in the anatomy of the normal human heart. *J. Gerontol*. 45(2):M33–M39, 1990.
[19]Koruth, J., *et al*. Direct assessment of catheter-tissue contact and RF lesion formation: a novel approach using endogenous NADH fluorescence. *Heart Rhythm*. S111, 2015.
[20]Lardo, A. C., *et al*. Visualization and temporal/spatial characterization of cardiac radiofrequency ablation lesions using magnetic resonance imaging. *Circulation* 102(6):698–705, 2000.
[21]Lee, G., P. Sanders, and J. M. Kalman. Catheter ablation of atrial arrhythmias: state of the art. *Lancet* 380(9852):1509–1519, 2012.
[22]Linte, C. A., J. J. Camp, M. E. Rettmann, D. R. Holmes, and R. A. Robb. Image-based modeling and characterization of rf ablation lesions in cardiac arrhythmia therapy. *Proc. SPIE–Int. Soc. Opt. Eng* 2013. doi:10.1117/12.2008529.
[23]Melby, S. J., *et al*. Atrial fibrillation propagates through gaps in ablation lines: implications for ablative treatment of atrial fibrillation. *Heart Rhythm* 5(9):1296–1301, 2008.
[24]Mercader, M., *et al*. Real-time NADH fluorescence imaging catheter (LuxCath): a novel imaging system for evaluation of radiofrequency ablation lesions and gaps. *Hear. Rhythm*. A-9102, 2013.
[25]Muselimyan, N., *et al*. Seeing the invisible: revealing atrial ablation lesions using hyperspectral imaging approach. *PLoS ONE* 11(12):e0167760, 2016.
[26]Oral, H., *et al*. Clinical significance of early recurrences of atrial fibrillation after pulmonary vein isolation. *J. Am. Coll. Cardiol*. 40(1):100–104, 2002.
[27]Reddy, V. Y., E. J. Schmidt, G. Holmvang, and M. Fung. Arrhythmia recurrence after atrial fibrillation ablation: can magnetic resonance imaging identify gaps in atrial ablation lines? *J. Cardiovasc. Electrophysiol*. 19(4):434–437, 2008.
[28]Roten, L., *et al*. Current hot potatoes in atrial fibrillation ablation. *Curr. Cardiol. Rev*. 8(4):327–346, 2012.
[29]Schwartzman, D., K. Schoedel, D. B. Stolz, and E. Di Martino. Morphological and mechanical examination of the atrial 'intima'. *Europace* 15(11):1557–1561, 2013.
[30]Singh-Moon, R. P., X. Yao, C. C. Marboe, and C. P. Hendon. Optical spectroscopy facilitated characterization of acute atrial lesions. *Biomed. Optics* 2016. doi: 10.1364/CANCER.2016.JTu3A.39.
[31]Swift, L., D. A. B. Gil, R. Jaimes, M. Kay, M. Mercader, and N. Sarvazyan. Visualization of epicardial cryoablation lesions using endogenous tissue fluorescence. *Circ. Arrhythm. Electrophysiol*. 7(5):929–937, 2014.
[32]Tsamis, A., J. T. Krawiec, and D. A. Vorp. Elastin and collagen fibre microstructure of the human aorta in ageing and disease: a review. *J. R. Soc. Interface* 10(83):20121004, 2013.
[33]Weerasooriya, R., *et al*. Catheter ablation for atrial fibrillation: are results maintained at 5 years of follow-up? *J. Am. Coll. Cardiol*. 57(2):160–166, 2011.